ADVANCED MATERIALS
www.advmat.de

www.MaterialsViews.com

Actively Tunable Visible Surface Plasmons in Bi_2Te_3 and their Energy-Harvesting Applications

*Meng Zhao, Jie Zhang, Nengyue Gao, Peng Song, Michel Bosman, Bo Peng, Baoquan Sun, Cheng-Wei Qiu, Qing-Hua Xu, Qiaoliang Bao, and Kian Ping Loh**

Surface plasmons arising from collective oscillations of conduction electrons have attracted intense research interest due to their promising applications in on-chip subwavelength electro-optical devices,[1] sensing,[2] and energy harvesting.[3] The broad goal of research in plasmonic materials is to design materials and structures with a tunable plasmon response. Highly doped semiconductors can be used as tunable plasmonic materials in the near-infrared regime by controlling the doping level.[4] Another widely studied tunable plasmonic material is graphene, which can sustain surface plasmon from far-infrared to mid-infrared regime.[5] While the plasmon resonance energy can be easily tuned by size and shape engineering, effective control of the plasmon resonance intensity, especially in the visible range, is challenging due to the lack of suitable plasmonic materials and modulation method. There are only limited demonstrations on the modulation of plasmonic resonance intensity, such as surface redox chemistry[6] and hydrogenation.[7] Identifying phase-change plasmonic materials that allow modulation would make an important step toward next-generation reconfigurable photonics and plasmonics devices.[8] It could also provide an important platform to study nanoscale light–matter interactions,[9] especially when the modulations can be achieved at the single-particle level or at the nanometer length scale.

As an excellent thermoelectric material,[10] Bi_2Te_3 has attracted renewed research interest since its discovery as a 3D topological insulator.[11] However, the most relevant applications of Bi_2Te_3 are currently in thermoelectrics,[12] and its 3D topological properties have largely remained as intellectual curiosities. We recently observed that Bi_2Te_3 hexagonal nanoplates can support multiple surface plasmon modes in the visible range, and are motivated to explore the application of this material.[13]

In this study, we have demonstrated that the plasmonic resonances in Bi_2Te_3 single-crystal nanoplates can be tuned in a wide spectral range by Se doping. Meanwhile, single-particle dark-field scattering spectroscopy and transmission electron microscopy (TEM)-based electron energy loss spectroscopy (EELS) were used here to show that the phase change between the crystalline and amorphous states in this material can efficiently control the intensity of the plasmon resonance. As opposed to collective response from an ensemble of particles, the phase change was observed at the nanoscale and at the single-nanoplate level. We further explored potential applications of this novel plasmonic material in energy harvesting and quantum-dot (QD) emission. The synthesized Bi_2Te_3 nanoplates were dispersed into a PEDOT:PSS films to fabricate hybrid solar cells with planar n-type silicon (n-Si). The plasmon resonances of Bi_2Te_3 in the visible range are found to strongly enhance the light absorption of silicon, resulting in a substantial increase of the short-circuit current. A Bi_2Te_3-incorporated Si/PEDOT:PSS hybrid solar cell achieved a high photoconversion efficiency (PCE) of 12.1%, with an improvement of 30% as compared to that of 9.3% for the reference device. The plasmonic effects of Bi_2Te_3 were also applied to plasmon-enhanced emission of quantum dots.

Single-crystalline Bi_2Te_3 nanoplates with a well-defined hexagonal shape were synthesized by the solvothermal method.[14] **Figure 1**a shows a scanning electron microscopy (SEM) image of the synthesized nanoplates, revealing a well-defined shape and a lateral dimensional dimension of 650 ± 200 nm. Atomic force microscopy (AFM) characterization (Figure 1b)

Dr. M. Zhao, Dr. N. Y. Gao, P. Song, Dr. B. Peng, Prof. Q.-H. Xu, Prof. K. P. Loh
Department of Chemistry
National University of Singapore
3 Science Drive 3, 117543, Singapore
E-mail: chmlohkp@nus.edu.sg
Dr. M. Zhao, P. Song, Dr. B. Peng, Prof. K. P. Loh
Centre for Advanced 2D Materials and Graphene Research Centre
National University of Singapore
6 Science Drive 2, 117546, Singapore
Dr. J. Zhang, Prof. B. Q. Sun, Prof. Q. L. Bao
Institute of Functional Nano and Soft Materials (FUNSOM)
Jiangsu Key Laboratory for Carbon-Based Functional Materials and Devices
and Collaborative Innovation Center of Suzhou Nano Science and Technology
Soochow University
Suzhou 215123, P. R. China
Dr. M. Bosman
Institute of Materials Research and Engineering
A*STAR (Agency for Science Technology and Research)
2 Fusionopolis Way 138634, Singapore
Dr. M. Bosman
Department of Materials Science and Engineering
National University of Singapore
9 Engineering Drive 1, 117575, Singapore
Prof. C.-W. Qiu
Department of Electrical and Computer Engineering
National University of Singapore
4 Engineering Drive 3, 117583, Singapore
Prof. Q. L. Bao
Department of Materials Science and Engineering
Faculty of Engineering
Monash University
Wellington road, Clayton 3800, Victoria, Australia

DOI: 10.1002/adma.201506367

© 2016 WILEY-VCH Verlag GmbH & Co. KGaA, Weinheim

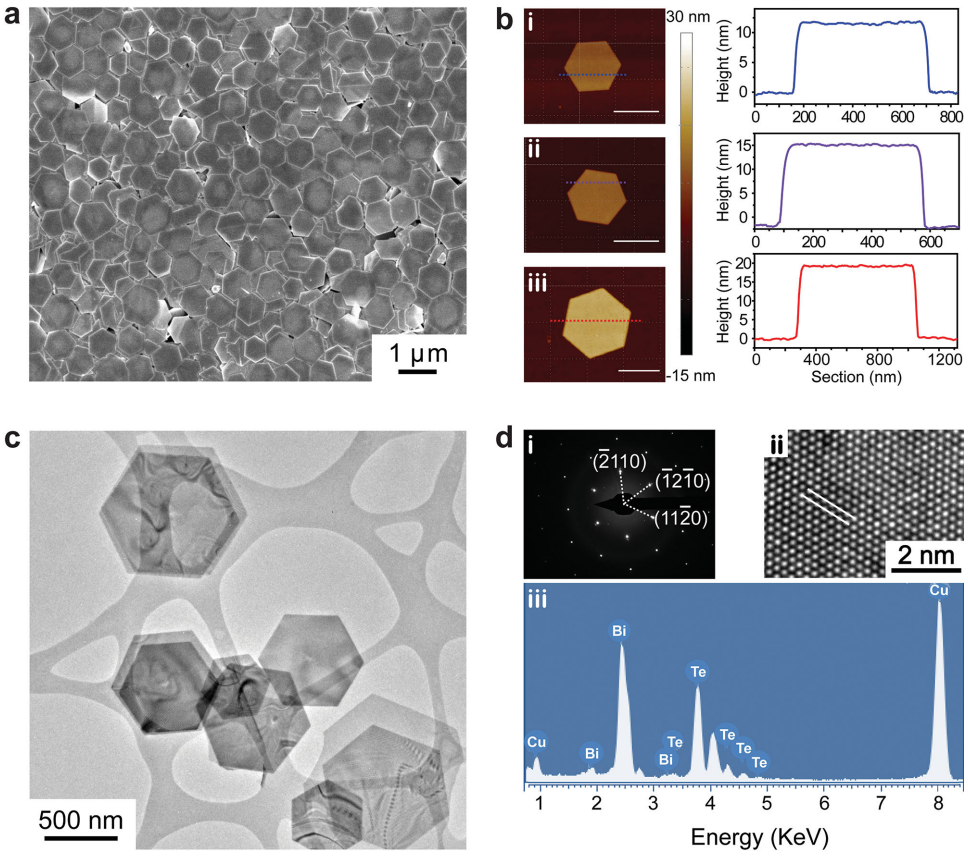

Figure 1. Microscopy characterizations of Bi_2Te_3 nanoplates. a) SEM image of the synthesized nanoplates. b) AFM images and corresponding height profiles of three typical nanoplates. Scale bar is 500 nm. c) TEM image of the nanoplates on a holey carbon support. d,i–iii) SAED pattern (i), HRTEM image (ii), and EDX spectrum (iii) of the synthesized nanoplates.

reveals that the Bi_2Te_3 nanoplates have very flat surfaces and an average thickness of 15 ± 5 nm. Figure 1c shows a representative TEM image of the hexagonal nanoplates, with ripple-like patterns as a result of the strain in the ultrathin structure. Sharp diffraction spots are observed in the selected area electron diffraction (SAED) pattern (Figure 1d(i)). High-resolution TEM (HRTEM) image (Figure 1d(ii)) shows a hexagonal atomic arrangement with lattice spacing of 0.22 nm. The microscopy characterizations prove that the synthesized nanoplates are high-quality single-crystal Bi_2Te_3. The nanoplate composition was confirmed by energy-dispersive X-ray (EDX) spectroscopy, yielding an elemental molar ratio of Bi to Te of ≈2:3, as shown in Figure 1d(iii).

The plasmonic response of Bi_2Te_3 nanoplates was investigated using multiple techniques. **Figure 2**a shows the UV–vis absorption spectra of the Bi_2Te_3 suspension in isopropyl alcohol (magenta line), where broad and significant absorption in the entire visible range is observed. To support surface plasmon resonances, the real part of the dielectric function (ε_1) of the material must be negative. Previous reports show that the cross-over frequency (at which ε_1 crosses zero) of Bi_2Te_3 is 1.6 eV, while the crossover frequency of Bi_2Se_3 is 2.2 eV.[15] The significant energy difference between the two compounds suggests a strategy to modulate the Bi_2Te_3 plasmon resonance energy by Se doping. The samples were synthesized by the solvothermal method and the value of x is determined with EDX (see Figure S1 in the Supporting Information). All the synthesized nanoplates exhibit a uniform size distribution similar to that of Bi_2Te_3 nanoplates. The doping effects were also evidenced by Raman spectroscopy (Figure S2, Supporting Information), which showed a systematic shift of the low-energy phonon modes. The plasmon absorption peaks were revealed in the UV–vis spectra of a series of $Bi_2Se_xTe_{3-x}$ samples. As shown in Figure 2a, all the samples show a strong broad absorption peak due to plasmonic resonances. The peak is broad due to the multiple plasmon modes and the inhomogeneous size distribution of the nanoplates in the solution. More importantly, we observed a clear blue shift of the resonance energy from 950 nm for $x = 0$ to 550 nm for $x = 3$, which is consistent with the shift of crossover frequency of ε_1 from Bi_2Te_3 to Bi_2Se_3. The plasmon resonance energy shift can be as wide as 400 nm after Se doping, which exceeds the range shown by novel plasmonic materials such as copper sulphide[4a] and tungsten oxide.[4c]

Bi_2Te_3 is well known as a phase-change material and a phase transition can be induced by various methods, including thermal treatment, laser illumination, and the application of an electric current.[16] By employing the crystalline–amorphous phase change, we achieved efficient modulation of its plasmon resonance intensity. The crystalline to amorphous phase change was realized by heating the sample at 390 °C for 3 min, followed by fast cooling to room temperature. In contrast, recrystallization could be achieved by slow heating/cooling process

© 2016 WILEY-VCH Verlag GmbH & Co. KGaA, Weinheim

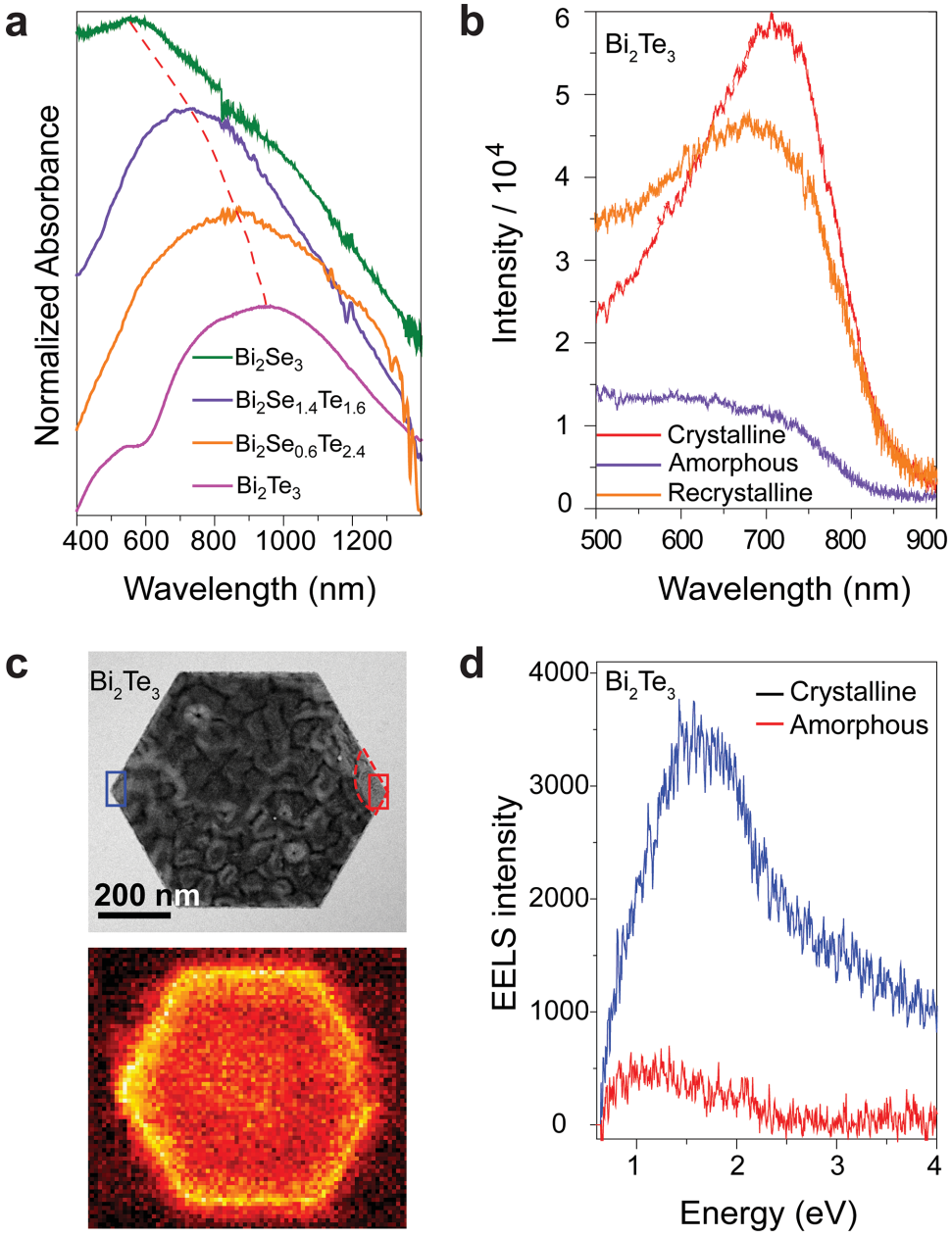

Figure 2. Modulations of Bi_2Te_3 surface plasmons. a) UV–vis spectra of $Bi_2Se_xTe_{3-x}$ samples show a clear shift with Se doping. b) Dark-field scattering spectra of a Bi_2Te_3 nanoplate at the three different stages after thermal treatments. c) TEM image and EELS map of a Bi_2Te_3 nanoplate with an amorphous corner, which is indicated by the red dashed line in the TEM image. EELS map was obtained by scanning a rectangular raster of pixels with the 1 nm electron probe and mapping the EELS counts in each pixel using an energy window of 0.1 eV. d) EELS spectrum from the crystal corner (blue rectangle in the TEM image) and from the amorphous corner (red rectangle in TEM image).

to/from 250 °C.[16] The corresponding changes in plasmon resonance were monitored by single-particle dark-field spectroscopy.[17] Figure 2b shows the dark-field scattering spectra of one typical Bi_2Te_3 nanoplate after different thermal treatments. Before heating, the pristine nanoplate showed plasmon resonance at ≈720 nm. After treatment at 390 °C, the plasmon peak intensity decreased by about 80% due to the amorphization of Bi_2Te_3 nanoplate. After recrystallization at 250 °C, the plasmon peak intensity was recovered to ≈75% of the original peak intensity. Similar observations were repeated for other Bi_2Te_3 nanoplates when subjected to the same phase-change treatments (Figure S3, Supporting Information). The energy shift between the UV–vis spectra and the dark-field scattering spectra is due to the difference in sampling an ensemble of nanoplates and a single nanoplate, respectively.

We further improved the resolution of our technique by using TEM–EELS to study the effects of the phase transition at the nanometer scale. Here, we intentionally identified a Bi_2Te_3 nanoplate with both crystalline and amorphous regions. Figure 2c shows a TEM image of a crystalline nanoplate with

© 2016 WILEY-VCH Verlag GmbH & Co. KGaA, Weinheim

an amorphous corner. The different crystallinity was confirmed by fast Fourier transform images, where no diffraction spot was observed in the amorphous corner, and six clear diffraction spots were observed in other part of the nanoplate (see Figure S4a,b, Supporting Information). Figure 2d shows the corresponding EELS map of the same nanoplate, where substantial intensity loss at the amorphous corner compared with other corners is observed. The monochromated EEL spectra from the amorphous corner and from the crystalline corner are shown in Figure 2d, clearly evidencing that the localized surface plasmons are manifested only in the crystalline regions. The phase transition leads to an intensity loss of 86% from crystalline to amorphous. We also identified a fully amorphous nanoplate where no obvious plasmon resonance was observed (Figure S4, Supporting Information). The ability to modulate the plasmon intensity at the single-particle level should have important relevance to future photonic and plasmonic applications.

Next, we studied possible plasmon-enhancement effects of the as-grown Bi_2Te_3 in a Si/PEDOT:PSS solar cell, the latter being an emerging high-performance, low-cost photovoltaic technology. In a Si/PEDOT:PSS hybrid solar cell, a Schottky junction is formed at the interface between Si and the PEDOT:PSS film. The difference between the work function of PEDOT:PSS and the conduction band of n-Si creates a built-in potential across the interface. Therefore, the generated charge carriers can be separated under the internal electrical field, and holes are collected and transferred by PEDOT:PSS film, while electrons go to the aluminum electrode directly. The PEDOT:PSS film not only acts as hole-transportation layer, but also plays an important role in collecting and transporting the generated charge carriers since the silver-grid top electrode covers only 10% of the surface area.

In this study, the as-synthesized Bi_2Te_3 nanoplates were blended with a PEDOT:PSS solution to form a composite, which was then spin-coated on planar n-doped Si to fabricate solar cells. **Figure 3**a shows a schematic illustration of the device structures. To optimize the performance of the Bi_2Te_3-incorporated Si/PEDOT:PSS solar cell, a series of test devices were prepared with different Bi_2Te_3 weight percentages of 0, 0.44%, 0.52%, 0.78%, 1.04%, and 1.30%, respectively. The performances of the fabricated devices were measured under illumination of AM 1.5 with an intensity of 100 mW cm^{-2}, and the results are summarized in Figure 3b. It is clear that the device performance can be significantly improved by incorporating Bi_2Te_3 into the polymer film. The PCE increases with increasing Bi_2Te_3 weight fraction, reaching the highest value of 12.1 % with 1.04 wt% Bi_2Te_3 added. However, further increase of the weight fraction of Bi_2Te_3 to 1.3 wt% results in a deterioration of the performance. Only nanoplates that are close to the interface would contribute

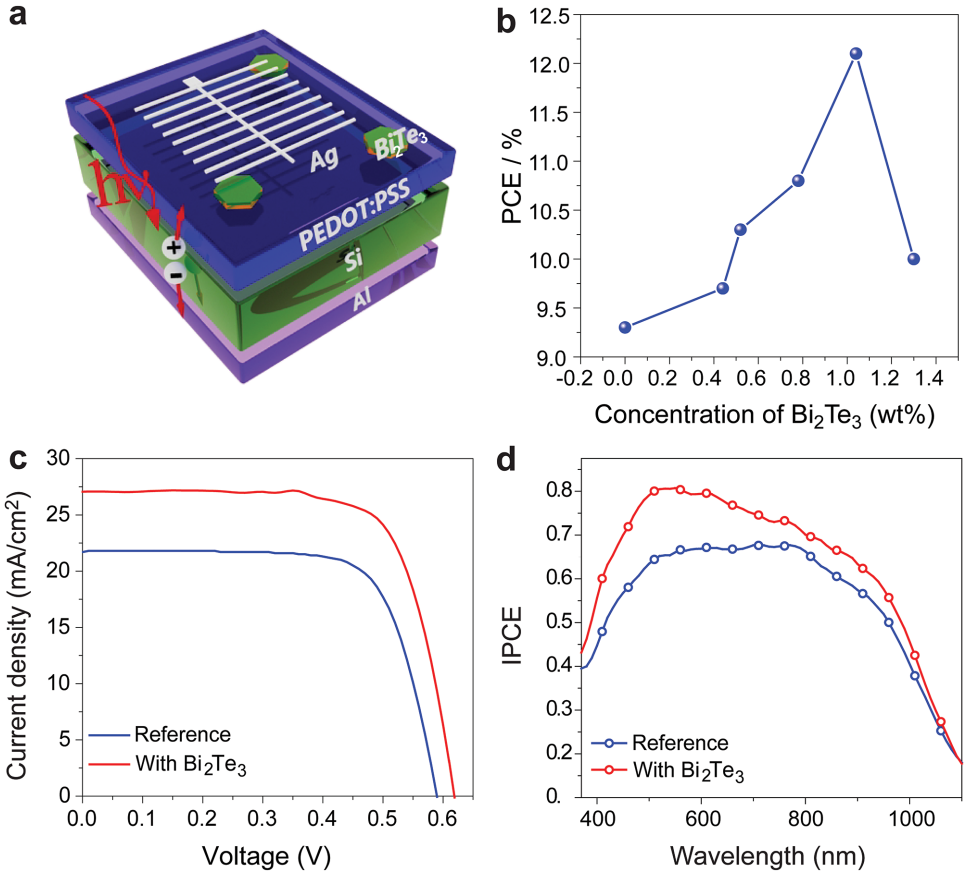

Figure 3. Surface-plasmon-enhanced performance of a solar cell due to Bi_2Te_3 incorporation. a) Schematic of the Bi_2Te_3-incorporated solar cell. b) Solar-cell PCE as a function of Bi_2Te_3 concentration. c,d) Current-density–voltage (*J*–*V*) characteristics (c) and IPCE (d) of devices with (1.04 wt%) and without Bi_2Te_3.

© 2016 WILEY-VCH Verlag GmbH & Co. KGaA, Weinheim

Table 1. Summary of the photovoltaic performance of solar cells with and without Bi_2Te_3.

Device	V_{oc} [V]	J_{sc} [mA cm^{-2}]	Fill factor	PCE [%]
Reference	0.59	21.75	0.72	9.3
With Bi_2Te_3	0.61	27.08	0.73	12.1

significantly to the PCE. Initially added Bi_2Te_3 nanoplates would increase the PCE due to their plasmonic effects. With the addition of excess Bi_2Te_3, light absorption and scattering by the nanoplates far away from the interface would reduce light absorption in the Si and thus lower the overall PCE.[18]

Figure 3c shows the current-density–voltage (J–V) characteristics of devices with (1.04 wt%) and without Bi_2Te_3. The detailed photovoltaic properties are summarized in **Table 1**. The performance of the Si/PEDOT:PSS hybrid solar cell with Bi_2Te_3 incorporated shows a significant improvement in the short-circuit current density (J_{sc}), from 21.75 mA cm^{-2} to 27.08 mA cm^{-2}, and the PCE was also much higher than that of the reference solar cell: 12.1 % compared to 9.3%. The increase of V_{oc} from 0.59 to 0.61 V is attributed to the increased Schottky barrier height due to introduction of Bi_2Te_3 nanoplates, as observed from dark-current measurements (see Figure S4, Supporting Information). It is worth noting that the PCE we achieved here is comparable to the best performing inorganic–organic (≈13%) solar cells in similar classes, obtained after optimization of electrode morphology and contacts.[19]

To investigate the wavelength dependence of the PCE in the Bi_2Te_3-enhanced hybrid solar cells, the incident photon-to-charge carrier efficiency (IPCE) of the hybrid solar cells (Figure 3d) was measured. A broadband enhancement of IPCE was observed for the Bi_2Te_3-incorporated solar cell, and there was a significant enhancement in the visible range. We attribute the enhanced absorption effects to the plasmon resonance in the Bi_2Te_3 hexagonal nanoplates. Surface plasmon resonances strongly enhance local electric fields and may create electron–hole pairs and improve light absorption near the Si layer.[3c] Besides the plasmonic effect, light scattering by the geometrical Bi_2Te_3 nanoplates can also enhance light absorption in Si, which can enhance IPCE in the short wavelength range (400–500 nm) away from the plasmon resonance energy. Such scattering-enhanced IPCE has been observed in metallic plasmonic nanostructures as well.[20]

The multiple plasmonic modes in Bi_2Te_3 nanoplates affect the performance of the solar cell in two ways: first, plasmonic light scattering increases the optical path length of incident light in the Si layer, which will result in more intense light absorption and excitons generation; second, the plasmon resonance enhances the optical–electrical field concentration, which was observed in previous EELS mapping and also verified by simulation in our previous study,[13] and thus improves light absorption. Under the condition of plasmon resonance, the scattering cross-section of Bi_2Te_3 nanoplates can be many times its geometric cross-section.[3a] The stronger light absorption of the Si layer induced by the Bi_2Te_3 can contribute to the improved short-circuit current density of the Bi_2Te_3-incorporated solar cell. Plasmon resonance could also increase the exciton dissociation probability as a result of local field enhancements.[21] Higher exciton dissociation results in a lower recombination rate, which would lead to the higher J_{sc} and fill factor observed in the Bi_2Te_3-incorporated solar cell.

Another important application of surface plasmons lies in their ability to enhance the spectral properties of fluorophores.[22] To investigate whether the surface plasmons of Bi_2Te_3 nanoplates can undergo radiative coupling with an optically emissive system, we studied the plasmonic effect of a single Bi_2Te_3 nanoplate on the fluorescence of CdSe/ZnS QDs. **Figure 4**a shows the schematic illustration of the sample structures. CdSe/ZnS QDs were chosen because they have an emission peak at 610 nm, which overlaps with the surface plasmon energy of Bi_2Te_3, and a monolayer film can be uniformly formed by self-assembly of these QDs (Figure 4b).[23] By manipulating the distance between the Bi_2Te_3 nanoplate and CdSe/ZnS QDs with Al_2O_3 as the dielectric spacer layer, the fluorescence can either be quenched or enhanced. The enhancement factor (EF) is defined as the ratio of I and I_0 (EF $= I/I_0$), where I and I_0 are the photoluminescence (PL) intensities of the CdSe/ZnS QDs monolayer with and without Bi_2Te_3, respectively. Figure 4c shows the PL intensity of QDs as a function of the thickness of the spacing layer. When the spacing layer is less than 10 nm, the fluorescence of QDs is quenched. The maximum fluorescence intensity is observed for QDs with a spacing layer of 20 nm, giving an EF of 3.8 (Figure 4d). The PL of QDs is a result of the competition of nonradiative and radiative rate. When the distance between Bi_2Te_3 and QDs is small (less than 10 nm in our case), nonradiative energy transfer from the QDs to Bi_2Te_3 is dominant and leads to PL quenching. With increasing separation distance, the nonradiative energy transfer is suppressed while absorption is enhanced due to local electric field[24] and the radiative rate is enhanced due to the Purcell effect,[25] leading to an enhancement of the PL. Further increase of the thickness (>20 nm) of the spacing layer leads to a decrease of the PL enhancement because both the local electric field and the Purcell effect become weaker. The enhancement of the PL by surface plasmon resonance is further proved by lifetime measurements. The time-resolved PL decay spectra were fitted with a biexponential function to derive the average lifetime.[23] The inset of Figure 4d shows the spacer-thickness-dependent lifetime of the QDs. The shortest lifetime is associated with the largest PL intensity when the spacer layer is 20 nm. The spacer-dependent PL lifetime is consistent with a previous study using Au nanorods as the plasmonic material.[23] In the plasmonics hybrid system, the plasmon–exciton coupling leads to increased radiative rate, which increases the intensity and decreases the lifetime of PL.[26] Regarding plasmon-enabled applications, the ability to tune the plasmon resonance of Bi_2Te_3 with Se doping would further broaden the applications of this novel plasmonic material.

In conclusion, we have demonstrated that the visible surface plasmons resonances in Bi_2Te_3 can be tuned in a wide range by Se doping. By employing the crystalline–amorphous phase transition, we achieved efficient modulation of the plasmon resonance intensity at both single-particle level and at the nanometer scale. Taking advantage of the multiple plasmon modes in Bi_2Te_3, which affords broadband absorption

© 2016 WILEY-VCH Verlag GmbH & Co. KGaA, Weinheim

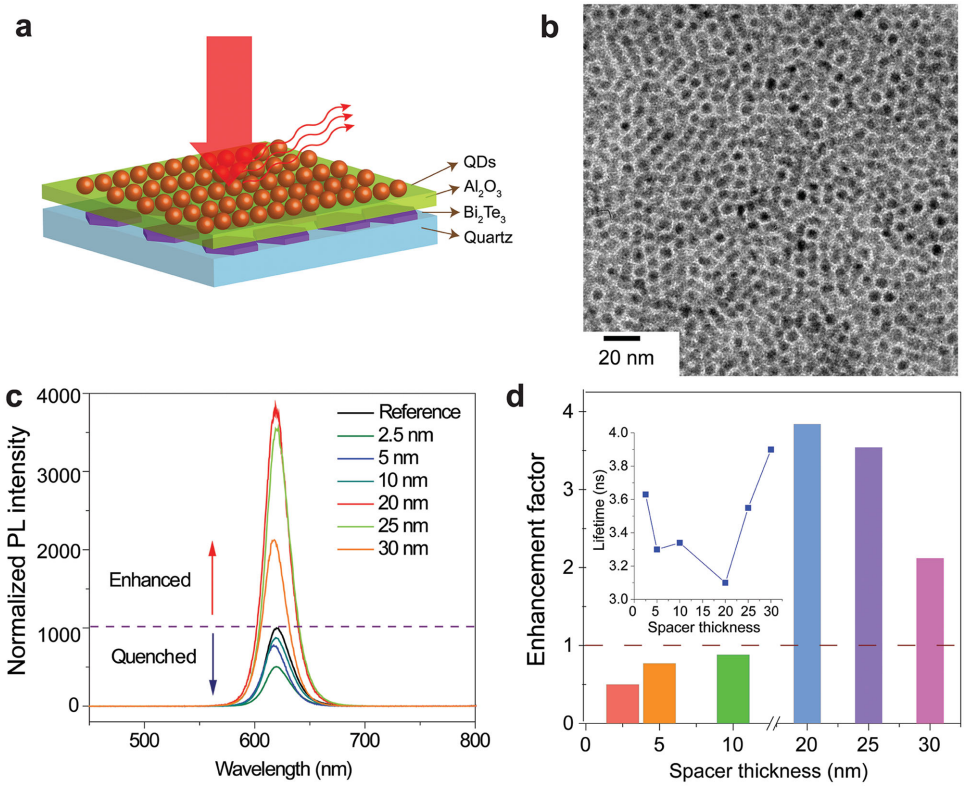

Figure 4. Manipulation of the emission of quantum dots with Bi_2Te_3 nanoplates. a) Schematics of the PL measurement. b) TEM image of self-assembly monolayer of CdSe/ZnS QDs. c,d) Normalized photoluminescence intensity (c) and enhancement factor (d) of quantum dots as a function of the thickness of the Al_2O_3 spacing layer between the single Bi_2Te_3 nanoplate and quantum dots. The inset is the spacer-thickness-dependent average PL lifetime.

in the visible range, we have used it to modify the interface of a Si/PEDOT:PSS hybrid solar cell and achieved a PCE of 12.1%, which represents an improvement of 30% for this class of solar cell. The capability of Bi_2Te_3 in manipulating the emission of quantum dots is also demonstrated and a fourfold emission enhancement can be achieved. Our observations suggest that Bi_2Te_3 nanoplates serve as a new class of tunable plasmonic material in the visible range and can be used to modulate nanoscale light–matter interactions in optoelectronic devices.

Supporting Information

Supporting Information is available from the Wiley Online Library or from the author.

Acknowledgments

K.P.L. and M.B. acknowledge the National Research Foundation funded CRP program "Plasmonic-Electronics: New Generation of Devices to Bypass Fundamental Limitations" (Award No. NRF-CRP 8-2011-07). C.-W.Q. acknowledges financial support from A*STAR Pharos Programme (Grant No. 152 70 00014, with Project No. R-263-000-B91-305). Q.L.B. acknowledges support from the youth 973 program (2015CB932700), the National Natural Science Foundation of China (Grant Nos. 91433107 and 51290273), and ARC DP (DP140101501). This work was performed in part at the Melbourne Centre for Nanofabrication (MCN) in the Victorian Node of the Australian National Fabrication Facility (ANFF).

Received: December 23, 2015
Revised: January 29, 2016
Published online: February 29, 2016

[1] M. I. Stockman, *Phys. Today* **2011**, *64*, 39.
[2] J. N. Anker, W. P. Hall, O. Lyandres, N. C. Shah, J. Zhao, R. P. Van Duyne, *Nat. Mater.* **2008**, *7*, 442.
[3] a) H. A. Atwater, A. Polman, *Nat. Mater.* **2010**, *9*, 205; b) B. J. Roxworthy, K. D. Ko, A. Kumar, K. H. Fung, E. K. C. Chow, G. L. Liu, N. X. Fang, K. C. Toussaint, *Nano Lett.* **2012**, *12*, 796; c) X. Dang, J. Qi, M. T. Klug, P.-Y. Chen, D. S. Yun, N. X. Fang, P. T. Hammond, A. M. Belcher, *Nano Lett.* **2013**, *13*, 637.
[4] a) J. M. Luther, P. K. Jain, T. Ewers, A. P. Alivisatos, *Nat. Mater.* **2011**, *10*, 361; b) M. M. Y. A. Alsaif, K. Latham, M. R. Field, D. D. Yao, N. V. Medehkar, G. A. Beane, R. B. Kaner, S. P. Russo, J. Z. Ou, K. Kalantar-zadeh, *Adv. Mater.* **2014**, *26*, 3931; c) K. Manthiram, A. P. Alivisatos, *J. Am. Chem. Soc.* **2012**, *134*, 3995.
[5] a) Z. Fei, A. S. Rodin, G. O. Andreev, W. Bao, A. S. McLeod, M. Wagner, L. M. Zhang, Z. Zhao, M. Thiemens, G. Dominguez, M. M. Fogler, A. H. C. Neto, C. N. Lau, F. Keilmann, D. N. Basov, *Nature* **2012**, *487*, 82; b) A. N. Grigorenko, M. Polini, K. S. Novoselov, *Nat. Photonics* **2012**, *6*, 749.
[6] Z. Li, J. J. Foley, S. Peng, C.-J. Sun, Y. Ren, G. P. Wiederrecht, S. K. Gray, Y. Sun, *Angew. Chem. Int. Ed.* **2015**, *54*, 8948.
[7] F. Sterl, N. Strohfeldt, R. Walter, R. Griessen, A. Tittl, H. Giessen, *Nano Lett.* **2015**, *15*, 7949.

© 2016 WILEY-VCH Verlag GmbH & Co. KGaA, Weinheim

[8] N. I. Zheludev, *Science* **2015**, *348*, 973.
[9] a) N. Rotenberg, L. Kuipers, *Nat. Photonics* **2014**, *8*, 919; b) J. A. Schuller, E. S. Barnard, W. Cai, Y. C. Jun, J. S. White, M. L. Brongersma, *Nat. Mater.* **2010**, *9*, 193.
[10] D. A. Wright, *Nature* **1958**, *181*, 834.
[11] D. Kong, Y. Cui, *Nat. Chem.* **2011**, *3*, 845.
[12] a) L.-P. Hu, T.-J. Zhu, Y.-G. Wang, H.-H. Xie, Z.-J. Xu, X.-B. Zhao, *NPG Asia Mater.* **2014**, *6*, e88; b) G. Zhou, D. Wang, *Sci. Rep.* **2015**, *5*, 8099.
[13] M. Zhao, M. Bosman, M. Danesh, M. Zeng, P. Song, Y. Darma, A. Rusydi, H. Lin, C.-W. Qiu, K. P. Loh, *Nano Lett.* **2015**, *15*, 8331.
[14] a) J. Song, F. Xia, M. Zhao, Y. L. Zhong, W. Li, K. P. Loh, R. A. Caruso, Q. Bao, *Chem. Mater.* **2015**, *27*, 3471; b) G. Zhang, W. Wang, X. Lu, X. Li, *Cryst. Growth Des.* **2009**, *9*, 145.
[15] J. Humlíček, D. Hemzal, A. Dubroka, O. Caha, H. Steiner, G. Bauer, G. Springholz, *Phys. Scr.* **2014**, *T162*, 014007.
[16] N. Han, S. I. Kim, J.-D. Yang, K. Lee, H. Sohn, H.-M. So, C. W. Ahn, K.-H. Yoo, *Adv. Mater.* **2011**, *23*, 1871.
[17] a) J. Kim, H. Son, D. J. Cho, B. Geng, W. Regan, S. Shi, K. Kim, A. Zettl, Y.-R. Shen, F. Wang, *Nano Lett.* **2012**, *12*, 5598; b) N. Gao, Y. Chen, L. Li, Z. Guan, T. Zhao, N. Zhou, P. Yuan, S. Q. Yao, Q.-H. Xu, *J. Phys. Chem. C* **2014**, *118*, 13904.
[18] E. S. Arinze, B. Qiu, G. Nyirjesy, S. M. Thon, *ACS Photonics* **2015**.
[19] a) Y. Zhang, F. Zu, S.-T. Lee, L. Liao, N. Zhao, B. Sun, *Adv. Energy Mater.* **2014**, *4*, 1300923; b) R. Liu, S.-T. Lee, B. Sun, *Adv. Mater.* **2014**, *26*, 6007; c) K.-T. Park, H.-J. Kim, M.-J. Park, J.-H. Jeong, J. Lee, D.-G. Choi, J.-H. Lee, J.-H. Choi, *Sci. Rep.* **2015**, *5*, 12093; d) P. Yu, C.-Y. Tsai, J.-K. Chang, C.-C. Lai, P.-H. Chen, Y.-C. Lai, P.-T. Tsai, M.-C. Li, H.-T. Pan, Y.-Y. Huang, C.-I. Wu, Y.-L. Chueh, S.-W. Chen, C.-H. Du, S.-F. Horng, H.-F. Meng, *ACS Nano* **2013**, *7*, 10780.
[20] S. Chang, Q. Li, X. Xiao, K. Y. Wong, T. Chen, *Energy Environ. Sci.* **2012**, *5*, 9444.
[21] F.-C. Chen, J.-L. Wu, C.-L. Lee, Y. Hong, C.-H. Kuo, M. H. Huang, *Appl. Phys. Lett.* **2009**, *95*, 013305.
[22] a) P. P. Pompa, L. Martiradonna, A. Della Torre, F. Della Sala, L. Manna, M. De Vittorio, F. Calabi, R. Cingolani, R. Rinaldi, *Nat. Nanotechnol.* **2006**, *1*, 126; b) W. Li, S. Wang, M. Hu, S. He, P. Ge, J. Wang, Y. Y. Guo, L. Zhaowei, *Sci. Rep.* **2015**, *5*, 11881; c) D. Lu, J. J. Kan, E. E. Fullerton, Z. Liu, *Nat. Nanotechnol.* **2014**, *9*, 48.
[23] B. Peng, Z. Li, E. Mutlugun, P. L. Hernandez Martinez, D. Li, Q. Zhang, Y. Gao, H. V. Demir, Q. Xiong, *Nanoscale* **2014**, *6*, 5592.
[24] P. Anger, P. Bharadwaj, L. Novotny, *Phys. Rev. Lett.* **2006**, *96*, 113002.
[25] a) F. Tam, G. P. Goodrich, B. R. Johnson, N. J. Halas, *Nano Lett.* **2007**, *7*, 496; b) K. Munechika, Y. Chen, A. F. Tillack, A. P. Kulkarni, I. Jen-La Plante, A. M. Munro, D. S. Ginger, *Nano Lett.* **2011**, *11*, 2725.
[26] a) S. T. Kochuveedu, T. Son, Y. Lee, M. Lee, D. Kim, D. H. Kim, *Sci. Rep.* **2014**, *4*, 4735; b) B. Peng, Q. Zhang, X. Liu, Y. Ji, H. V. Demir, C. H. A. Huan, T. C. Sum, Q. Xiong, *ACS Nano* **2012**, *6*, 6250.

© 2016 WILEY-VCH Verlag GmbH & Co. KGaA, Weinheim